The Magnetothermal Instability (MTI) and Its Role in the Transport of Angular Momentum in Hot, Dilute, Magnetized Accretion

Tanim Islam

École Normale Supérieure
University of Virginia

CENTRE NATIONAL DE LA RECHERCHE SCIENTIFIQUE

l'Observatoire de Paris

RESULTS

Modal Analysis

Modal analysis of the collisionless MTI and MVTI:

- Axisymmetric nonradial perturbations, $\delta A \propto \exp\left(\Gamma t + ik_Z z\right)$, Γ the growth rate, k_Z the vertical wavenumber.
- **Fluid** approach applicable in the outer disk, where ion and electron temperatures are the same; fixed Prandtl number $\mathrm{Pr} = \eta_k/\eta_\nu \approx 1/101$.
- Fluid treatment is done in the incompressible limit; kinetic treatment necessarily includes finite compressibility (small imaginary part to growth rate).

Full perturbed particle distribution functions (for collisionless and mildly collisional MTI)

Perturbed ion and electron distribution function for collisionless MHD in a rotating frame,

$$
\begin{aligned}
&\left(\Gamma + ik_\parallel v_\parallel + \nu_i\right)\delta f_i - \frac{\partial \delta f_i}{\partial v_\parallel}\left(\frac{k_B T_{i0}}{m_p}\times\frac{z}{H^2}\sin\chi\right) = \frac{m_p v_\parallel}{k_B T_{i0}}\left(-ik_\parallel \mu\delta B + \frac{e\delta E_\parallel}{m_p} - \right.\\
&\left.\frac{z}{H^2}v_i^2 v_\parallel \delta b_Z + v_i^2\frac{\partial \ln p_{i0}}{\partial R}\delta\bar{B}_R - \frac{\cos\chi\delta\bar{B}_R}{ik_\parallel}\left(\Omega' R\left[\Gamma + ik_\parallel v_\parallel\right] + 2\Omega\Gamma\right)\right) f_{i0}' + \\
&\nu_i f_{i0}'\left(\delta\bar{\rho} - \frac{\delta T_{i\parallel}/2 + \delta T_{i\perp}}{T_{i0}} + \left[\frac{m_p\mu B_0}{k_B T_{i0}} + \frac{m_p v_\parallel^2}{2k_B T_{i0}}\right]\left[\frac{\delta T_{i\parallel}/3 + 2\delta T_{i\perp}/3}{T_{i0}}\right] - \right.\\
&\left.\frac{m_p\mu\delta B}{k_B T_{i0}} + \frac{m_p v_\parallel \delta v_\parallel}{k_B T_{i0}}\right) - f_{i0}'\left(v_\parallel\delta\mathbf{b} + \delta\mathbf{u}_\perp\right)\cdot\left(\frac{\partial \ln\rho_0}{\partial R}\hat{\boldsymbol{R}} - \frac{z\hat{\boldsymbol{z}}}{H^2} - \frac{3}{2}\frac{\partial \ln T_{i0}}{\partial R}\hat{\boldsymbol{R}} + \right.\\
&\left.\left(\frac{m_p\mu B_0}{k_B T_{i0}} + \frac{m_p v_\parallel^2}{2k_B T_{i0}}\right)\frac{\partial \ln T_{i0}}{\partial R}\hat{\boldsymbol{R}}\right),
\end{aligned}
\tag{1}
$$

$$
\begin{aligned}
&\left(\Gamma + ik_\parallel v_\parallel + \nu_e\right)\delta f_e - \frac{\partial \delta f_e}{\partial v_\parallel}\left(\frac{k_B T_{e0}}{m_e}\times\frac{z}{H^2}\sin\chi\right) = \frac{m_e v_\parallel}{k_B T_{e0}}\left(-ik_\parallel \mu\delta B - \frac{e\delta E_\parallel}{m_e} - \right.\\
&\left.\frac{z}{H^2}v_e^2 v_\parallel \delta b_Z + v_e^2\frac{\partial \ln p_{e0}}{\partial R}\delta\bar{B}_R - \frac{\cos\chi\delta\bar{B}_R}{ik_\parallel}\left(\Omega' R\left[\Gamma + ik_\parallel v_\parallel\right] + 2\Omega\Gamma\right)\right) f_{e0}' + \\
&\nu_e f_{e0}'\left(\delta\bar{\rho} - \frac{\delta T_{e\parallel}/2 + \delta T_{e\perp}}{T_{e0}} + \left[\frac{m_e\mu B_0}{k_B T_{e0}} + \frac{m_e v_\parallel^2}{2k_B T_{e0}}\right]\left[\frac{\delta T_{e\parallel}/3 + 2\delta T_{e\perp}/3}{T_{e0}}\right] - \right.\\
&\left.\frac{m_e\mu\delta B}{k_B T_{e0}} + \frac{m_e v_\parallel \delta v_\parallel}{k_B T_{e0}}\right) - f_{e0}'\left(v_\parallel\delta\mathbf{b} + \delta\mathbf{u}_\perp\right)\cdot\left(\frac{\partial \ln\rho_0}{\partial R}\hat{\boldsymbol{R}} - \frac{z\hat{\boldsymbol{z}}}{H^2} - \frac{3}{2}\frac{\partial \ln T_{e0}}{\partial R}\hat{\boldsymbol{R}} + \right.\\
&\left.\left(\frac{m_e\mu B_0}{k_B T_{e0}} + \frac{m_e v_\parallel^2}{2k_B T_{e0}}\right)\frac{\partial \ln T_{e0}}{\partial R}\hat{\boldsymbol{R}}\right).
\end{aligned}
\tag{2}
$$

We denote terms in dark red with finite collisionality, terms in dark green with points away from the midplane, terms in purple with differential rotation, and terms in dark blue with radial equilibrium gradients in pressure and temperature.

MVTI Dispersion Relations

On top is the MRI-like dispersion relation, and on the bottom is the MVI-like dispersion relation, for the MVTI. We take $\alpha_P = 10$ and choose various $\alpha_T \geq 0$ such that the system is Schwarzchild stable.

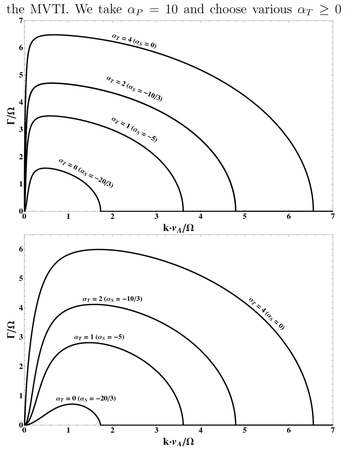

Plot of the MVTI dispersion relation for $\eta_b\Omega/v_A^2 = 10^2$.

Plot of the MVTI dispersion relation for $\eta_b\Omega/v_A^2 = 1$.

Collisionless MTI Dispersion Relation

- Real part of the collisionless MTI dispersion relation appears qualitatively similar to the MVTI. Collisionless damping of long-wavelength modes with phase velocities of the order sound speed, $k_\parallel \lesssim \Omega\theta_0^{1/2}$. We choose $\beta = 10^2$.

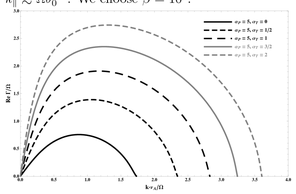

Real part of the dispersion relation of the collisionless MTI for $\alpha_P = 5$ and $\alpha_T > 0$ such that the system is Schwarzchild stable.

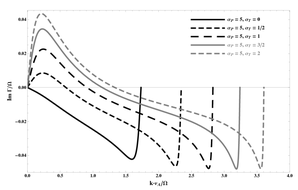

Imaginary part of the dispersion relation of the collisionless MTI for $\alpha_P = 5$ and $\alpha_T > 0$ such that the system is Schwarzchild stable.

- As $\beta \to 1$, the collisionless fluxes of momentum and viscosity become dynamically unimportant, and the collisionless MTI becomes more incompressible. Similar behavior has been observed by [20] for the collisionless MRI.

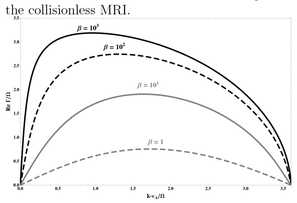

Real part of the collisionless MTI dispersion relation for $\alpha_P = 5$, $\alpha_T = 2$, and varying $\beta \geq 1$.

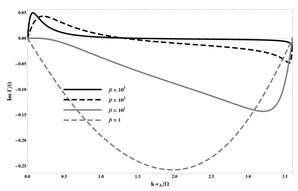

Imaginary part of the collisionless MTI dispersion relation for $\alpha_P = 5$, $\alpha_T = 2$, and varying $\beta \geq 1$.

Quadratic Fluxes for MVTI

Quadratic angular momentum flux, MRI-like mode

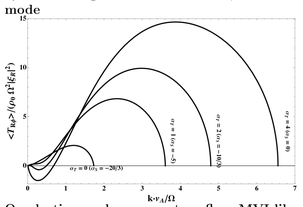

Quadratic heat flux, MRI-like mode

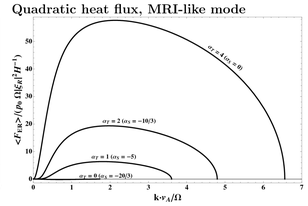

Quadratic angular momentum flux, MVI-like mode

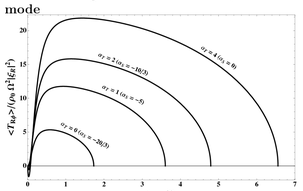

Quadratic heat flux, MVI-like mode

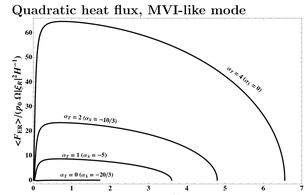

Quadratic Fluxes for Collisionless MTI

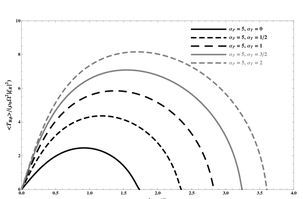

Normalized $\langle T_{R\phi}\rangle$ for the collisionless MTI, $\beta = 10^2$, $\chi = \pi/4$, $\alpha_P = 5$, and $0 \leq \alpha_T \leq 2$.

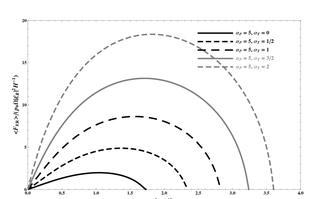

Normalized $\langle q_R\rangle$ for the collisionless MTI, $\beta = 10^2$, $\chi = \pi/4$, $\alpha_P = 5$, and $0 \leq \alpha_T \leq 2$.

Normalized quadratic angular momentum flux for the collisionless MRI, $1 \leq \beta \leq 10^4$. As $\beta \to 1$, we reduce to the classical MRI.

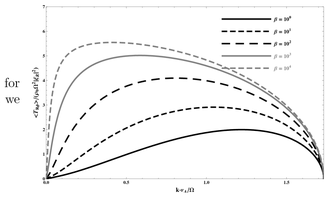

Mildly Collisional MTI Dispersion Relation

For weakly magnetized plasmas, we reduce to the fluid approximation for $\nu_i \gtrsim \Omega\beta^{1/2}$ – i.e., when the wavelength of the fastest growing mode $\gtrsim \lambda_i$, the ion collisional mean free path [21].

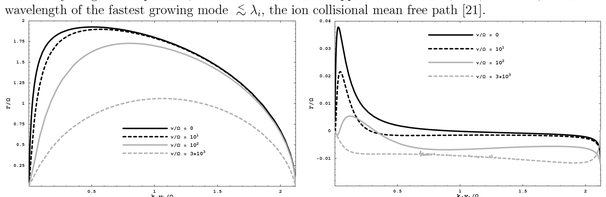

Real (left) and imaginary (right) parts of the growth rate of the midlly collisional MTI. We reproduce the MVTI dispersion relation for $\nu_i \geq \Omega\beta^{1/2}$.

Unresolved Points

Normalized angular momentum flux for the MVTI in a rigidly rotating ($\Omega' R = 0$) disk. Phenomenological analysis, of a radial disk slice near marginal stability to the MVTI or collisionless MTI at high Reynolds numbers, as done by [22] in their analysis of hydrodynamic stability of different rotational profiles, may be required to understand the nature of angular momentum transport in the saturated MVTI.

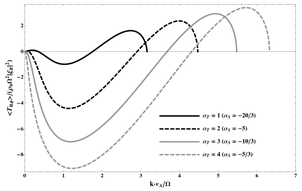

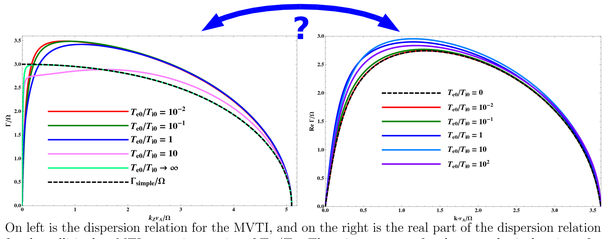

On left is the dispersion relation for the MVTI, and on the right is the real part of the dispersion relation for the collisionless MTI, at various ratios of T_{e0}/T_{i0}. There is agreement for the astrophysical regimes for RIAFs, $T_{i0} \gtrsim T_{e0}$, but not for the case $T_{e0} \gg T_{i0}$. To resolve this issue may involve analyzing the mildly collisional MTI, including both ion and electron collisionality.

In order to analyze the dynamics of collisionless MHD modes away from the midplane, we require solutions to the following equation:

$$
\left(y - i\zeta\right) f_n\left(y\right) + i\hat{z}\frac{df_n}{dy} = \pi^{-1/2} y^n e^{-y^2}
$$

where $\hat{z}$ is a normalized height. Integrals, $Z_n\left(\zeta, \hat{z}\right) = \int_{-\infty}^{\infty} f_n\left(y\right) dy$, need to be evaluated. In the limit $\hat{z} = 0$, these reduce to the plasma response function.

Shown below are dispersion relations for the collisionless offplane MRI:

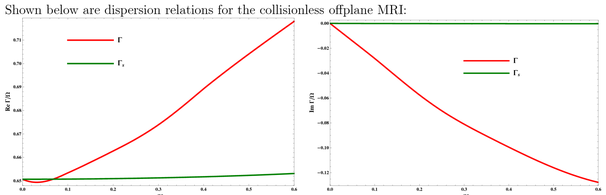

At left is the real, and at right is the imaginary, normalized growth rate as a function of height z/H for $k_Z v_{A0}/\Omega = 10^{-1}$.

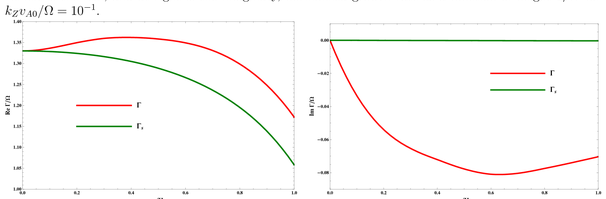

At left is the real, and at right is the imaginary, normalized growth rate as a function of height z/H for $k_Z v_{A0}/\Omega = 1$. We compare Γ to Γ_s.
These calculations are extremely computationally expensive. Some ingenuity might be needed to solve the growth rate as a function of wavenumber more efficiently.

FURTHER RESEARCH

Landau Fluid Closures

Landau fluid closures of higher-order moments of the distribution function, which are typically expressions for the heat fluxes, are employed in order to model the appropriate physics of a collisionless plasma using a fluid formalism. The fluid closure heat fluxes $q_\perp$ and $q_\parallel$ match their respective collisionless heat fluxes to various orders in the growth rate Γ. These closures are chosen to satisfy conservation laws, such as density, momentum, and energy. They have been used in the study of ion temperature gradient modes [23, 24, 25], gyrokinetic plasmas [26, 27], and collisionless MHD plasmas [28].

Forms of $\delta q_\parallel$ and $\delta q_\perp$ that match the collisionless MHD forms of $\delta q_\parallel$ and $\delta q_\perp$ best:

$$
\begin{aligned}
\frac{\delta q_\parallel}{p_{i0} v_i} = &\; 2i\sqrt{\frac{2}{\pi}}\left(\frac{\delta\rho}{\rho_0} - \frac{\delta p_\parallel}{p_{i0}}\right) - \\
&2\left(\frac{1}{k_\parallel}\frac{\partial \ln T_0}{\partial R}\right)\sqrt{\frac{2}{\pi}}\frac{\delta B_R}{B_0} \\
\frac{\delta q_\perp}{p_{i0} v_i} = &\; i\sqrt{\frac{2}{\pi}}\left(\frac{\delta p}{\rho_0} - \frac{\delta p_\perp}{p_{i0}}\right) - \\
&\left(\frac{1}{k_\parallel}\frac{\partial \ln T_{i0}}{\partial R}\right)\sqrt{\frac{2}{\pi}}\frac{\delta B_R}{B_0}
\end{aligned}
$$

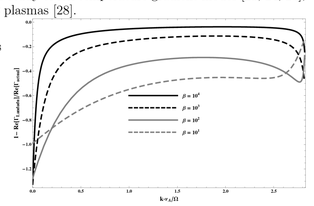

Comparison of the relative differences between the real part of the "Landau" and "exact" expressions for the growth rate, defined as $1 - \mathrm{Re}\left(\Gamma_{\mathrm{Landau}}\right)/\mathrm{Re}\left(\Gamma_{\mathrm{exact}}\right)$.

Pressure Anisotropy Instabilities

MHD Anisotropizing Instability

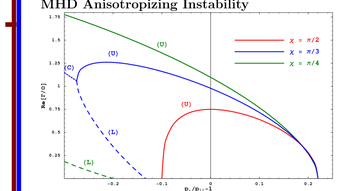

Demonstration of additional instabilities arising from equilibrium pressure anisotropy. We take $\beta = 10$, purely vertical wavenumber $k_\parallel v_A/\Omega = \sqrt{15}/4$, and plot the real part of the growth rate. Note that for the MRI, all solutions of equilibrium magnetic fields that are not purely vertical become MHD-stabilized at $p_{\perp 0}/p_{\parallel 0} - 1 \sim \beta^{-1}$.

Gyrokinetic Isotropizing Instabilities

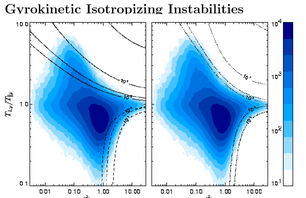

Pressure anisotropy, easily excited in collisionless plasmas, may lead to an astrophysical flow in which $|p_\parallel/p_\perp|/p \sim \beta^{-\alpha}$, where $\alpha \sim 1$, due to gyrokinetic firehose/mirror instabilities. Above figure is a density histogram of measurements of the solar wind by the WIND telescope, and is taken from [29].

Necessity of Global Simulations?

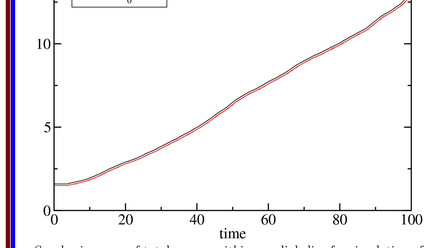

Secular increase of total energy within a radial slice for simulation of the MRI. Figure taken from [30].

Global simulations are **necessary** for modeling radiatively inefficient flows; codes that explicitly conserve all energy, such as Athena [30], are necessary to model the nonlinear rotational MTI.

BUT...Only Local Numerical Simulations Computationally Accessible?

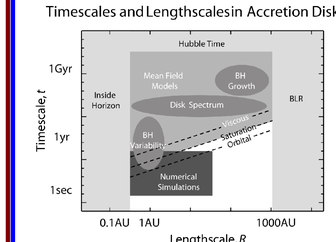

The dynamic spatial and temporal range of observations and numerical simulations of central supermassive black hole accretion processes. Even with state-of-the-art computational resources, there is significant disjoint between phenomena that can be explored numerically and that can be observed. This requires that the nature of local turbulence in RIAFs be explored in detail, in order to characterize the nature of angular momentum transport and heat flux due to the nonlinear saturated MVTI or collisionless MTI. This figure is taken from [31] (M. Pessah, Astronomy Thesis, University of Arizona [2007]).